

SOLAR CELLS

Perovskite solar cells with CuSCN hole extraction layers yield stabilized efficiencies greater than 20%

Neha Arora,^{1*} M. Ibrahim Dar,^{1,*†} Alexander Hinderhofer,² Norman Pellet,¹ Frank Schreiber,² Shaik Mohammed Zakeeruddin,¹ Michael Grätzel^{1†}

Perovskite solar cells (PSCs) with efficiencies greater than 20% have been realized only with expensive organic hole-transporting materials. We demonstrate PSCs that achieve stabilized efficiencies exceeding 20% with copper(I) thiocyanate (CuSCN) as the hole extraction layer. A fast solvent removal method enabled the creation of compact, highly conformal CuSCN layers that facilitate rapid carrier extraction and collection. The PSCs showed high thermal stability under long-term heating, although their operational stability was poor. This instability originated from potential-induced degradation of the CuSCN/Au contact. The addition of a conductive reduced graphene oxide spacer layer between CuSCN and gold allowed PSCs to retain >95% of their initial efficiency after aging at a maximum power point for 1000 hours under full solar intensity at 60°C. Under both continuous full-sun illumination and thermal stress, CuSCN-based devices surpassed the stability of spiro-OMeTAD-based PSCs.

The tailoring of the formation and composition of the absorber layer in organic-inorganic perovskite solar cells (PSCs) has resulted in certified power conversion efficiencies (PCEs) exceeding 20% (1, 2). These PCEs have been obtained while retaining the electron-selective TiO₂ layer and by using either spiro-OMeTAD [2,2',7,7'-tetrakis(*N,N*-di-*p*-methoxyphenyl-amine)9,9'-spiro-bifluorene] or a polymer-based poly(triarylamine) (PTAA) as the hole-transporting material (HTM) (2, 3). However, the cost of these HTMs is prohibitively high for large-scale applications, and the archetype organic HTMs or their ingredients apparently are a factor in the long-term operational and thermal instability of the PSCs that use them (4). One strategy to combat these issues of cost and instability could be the use of inexpensive inorganic hole extraction layers, similar to the use of TiO₂ as an electron-transporting material (5). However, obtaining stable PCEs of >20% with PSCs that use inorganic HTMs (such as NiO, CuI, Cs₂SnI₆, and CuSCN) when subjected to light soaking under realistic operational conditions (i.e., at maximum power point and 60°C) has remained a challenge (6–9).

The realization of efficiencies of >20% from PSCs using inorganic HTMs remains a key goal that would foster the large-scale deployment of PSCs. Among various inorganic HTMs, CuSCN is an extremely cheap, abundant p-type semiconductor that exhibits high hole mobility, good thermal stability, and a well-aligned work func-

tion (10). It is intrinsically p-doped and transmits light across the entire visible and near-infrared spectral region, so it is also attractive for tandem cell applications where the PSC is placed on top of a semiconductor with a lower band gap (11). However, the stabilized PCE values reported with CuSCN lag far behind devices based on the standard spiro-OMeTAD. CuSCN deposition methods including doctor blading, electrodeposition, spin coating, and spray coating have been tried (9, 12–16). Of these, the solution-based bottom-up approaches are more facile; however, a critical issue associated with them is that most of the solvents in which CuSCN shows high solubility degrade the perovskite layer (17). Because of the dearth of solvents that readily dissolve CuSCN but not the perovskites, an inverted device architecture has been used, albeit with moderate success (12).

To retain the mesoscopic TiO₂-based normal device architecture, we developed a simple dynamic deposition method. Typically, we deposited a thin and uniform CuSCN layer on top of a CsFAMAPbI_{3-x}Br_x [FA = CH(NH₂)₂⁺, MA = CH₃NH₃⁺] perovskite layer. To do so without compromising the quality of the perovskite layer, we drop-cast a defined volume of CuSCN dissolved in diethyl sulfide (DES, 35 mg/ml) in 2 to 3 s while spinning the substrate at 5000 rpm (18). The structural features of this CuSCN layer were investigated by x-ray diffraction (XRD). CuSCN crystallizes generally in two polymorphs, α -CuSCN (19) and β -CuSCN (20, 21), where the latter exhibits polytypism (i.e., variation in layer stacking order). A comparison of the calculated powder XRD spectra and grazing incidence XRD data of CuSCN (Fig. 1A) shows that the dynamic deposition method yielded β -CuSCN. A broad reflection at $q = 1.9 \text{ \AA}^{-1}$ established the presence of different polytypes of β -CuSCN, predom-

inantly 2H and 3R. Coherently scattering island sizes of 17 and 18 nm were estimated from the peak width of the (002) reflection of CuSCN deposited, respectively, on the glass and the perovskite film. To determine the domain orientation, we acquired grazing incidence wide-angle x-ray scattering (GIWAXS) data from CuSCN and CuSCN/perovskite films (Fig. 1, B and C). The intensity distribution of the (002) β -CuSCN ring (fig. S1) reveals that the CuSCN domains have preferential orientation, with the long unit cell axis parallel to the substrate (Fig. 1, D and E).

Scanning electron microscopy (SEM) images of the perovskite film acquired before (Fig. 2A) and after (Fig. 2B) the deposition of a CuSCN layer revealed the homogeneous coverage of the perovskite overlayer with the CuSCN layer. By comparison, for a spiro-OMeTAD layer deposited via the conventional spin-coating method, the presence of pinholes was evident (fig. S2), which could be detrimental to performance (22). To evaluate the thickness of various layers, we acquired a cross-sectional SEM image (Fig. 2C) of the complete device, which established the formation of a thin CuSCN layer (~60 nm) sandwiched between a perovskite overlayer and a gold layer. Because DES is a strong solvent, it could damage the underlying perovskite layer (fig. S3). Thus, we used a dynamic deposition approach in which the solvent evaporated more rapidly than in conventional deposition.

To investigate the charge carrier dynamics in pristine and HTM-containing perovskite films, we used steady-state photoluminescence (PL) and time-correlated single-photon counting (TCSPC) spectroscopy. The pristine perovskite film exhibited an intense PL emission centered around 773 nm with a linewidth of 44 nm (Fig. 2D). In the presence of a charge extraction layer, the PL of the pristine perovskite film was strongly quenched, from which very rapid extraction of electrons or holes across the interfaces could be inferred (23). We used TCSPC spectroscopy to estimate the dynamics of charge carriers quantitatively (Fig. 2E). The long lifetime of the charge carriers ($\tau_{10} = 390 \text{ ns}$) is indicative of the high electronic quality of the pristine perovskite film (τ_{10} is the time at which the initial PL intensity decreases by a factor of 10) (24). In agreement with the steady-state PL, the charge carrier lifetime decreased sharply in the perovskite films containing TiO₂ ($\tau_{10} = 49 \text{ ns}$) as the electron extraction layer and spiro-OMeTAD ($\tau_{10} = 22 \text{ ns}$) or CuSCN ($\tau_{10} = 16 \text{ ns}$) as the hole extraction layer (25). In comparison, the hole injection from the valence band of perovskite into the highest occupied molecular orbital (HOMO) or valence band of HTM was more rapid than the electron injection from the conduction band of perovskite into that of TiO₂ (26). In addition, TCSPC spectroscopy showed that the hole transfer was faster across the perovskite-CuSCN junction relative to the perovskite-spiro-OMeTAD interface, although the thermodynamic driving force (difference between the two energy levels) is lower at the perovskite-CuSCN interface (27). This difference could be explained by considering that

¹Laboratory of Photonics and Interfaces, Department of Chemistry and Chemical Engineering, Ecole Polytechnique Fédérale de Lausanne (EPFL), CH-1015 Lausanne, Switzerland. ²Institut für Angewandte Physik, Universität Tübingen, 72076 Tübingen, Germany.

*These authors contributed equally to this work.

†Corresponding author. Email: ibrahim.dar@epfl.ch (M.I.D.); michael.gratzel@epfl.ch (M.G.)

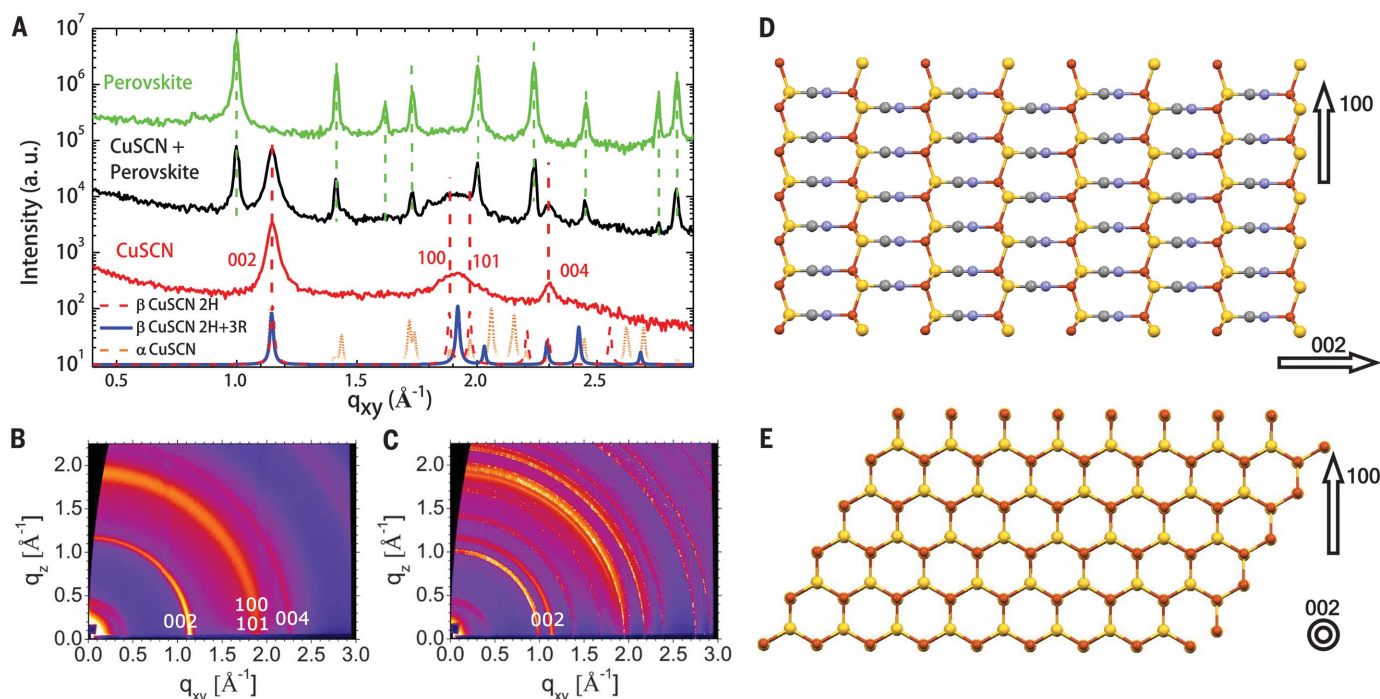


Fig. 1. Structural characterization of CuSCN films coated on glass or perovskite. (A) Grazing incidence XRD data acquired from a pure CuSCN film coated on glass, CuSCN coated on perovskite/TiO₂/fluorine-doped tin oxide (FTO), and bare perovskite/TiO₂/FTO. At the bottom, calculated powder diffraction data from CuSCN are shown for comparison. Indexing of the CuSCN pattern is performed according to the CuSCN 2H β -structure. (B) GIWAXS

data obtained from a CuSCN film coated on a glass substrate. (C) GIWAXS data obtained from a CuSCN film coated on a perovskite layer. In (C), the (002) reflection is visible; other reflections are superimposed with more intense reflections from the perovskite film. (D and E) The preferential out-of-plane orientation of CuSCN (the in-plane orientation is rotated by 90°). Color code: red, copper atoms; yellow, sulfur atoms; gray, carbon atoms; blue, nitrogen atoms.

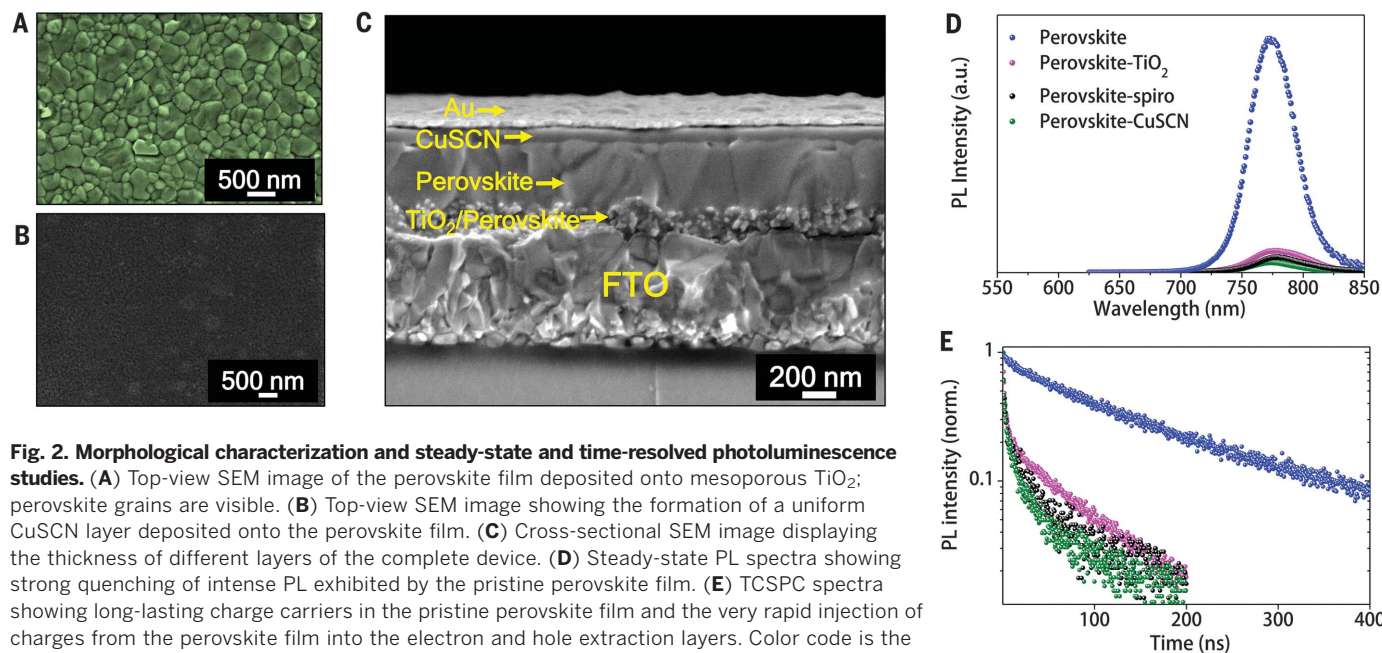


Fig. 2. Morphological characterization and steady-state and time-resolved photoluminescence studies. (A) Top-view SEM image of the perovskite film deposited onto mesoporous TiO₂; perovskite grains are visible. (B) Top-view SEM image showing the formation of a uniform CuSCN layer deposited onto the perovskite film. (C) Cross-sectional SEM image displaying the thickness of different layers of the complete device. (D) Steady-state PL spectra showing strong quenching of intense PL exhibited by the pristine perovskite film. (E) TCSPC spectra showing long-lasting charge carriers in the pristine perovskite film and the very rapid injection of charges from the perovskite film into the electron and hole extraction layers. Color code is the same as in (D).

there are stronger interfacial interactions between the perovskite and CuSCN than between the perovskite and the organic layer.

Apart from injection, the transport of charges through the HTM layer is another critical process

that strongly influences overall device performance. In fully assembled devices, hole mobilities of $1.4 \times 10^{-6} \text{ cm}^2 \text{ V}^{-1} \text{ s}^{-1}$ and $1.2 \times 10^{-3} \text{ cm}^2 \text{ V}^{-1} \text{ s}^{-1}$ were assessed for spiro-OMeTAD and CuSCN, respectively, by using photo charge extraction

and linearly increasing voltage. With similar charge separation and recombination dynamics in the perovskite, CuSCN's higher hole mobility (by about three orders of magnitude) and thinner layer offer a distinct advantage over

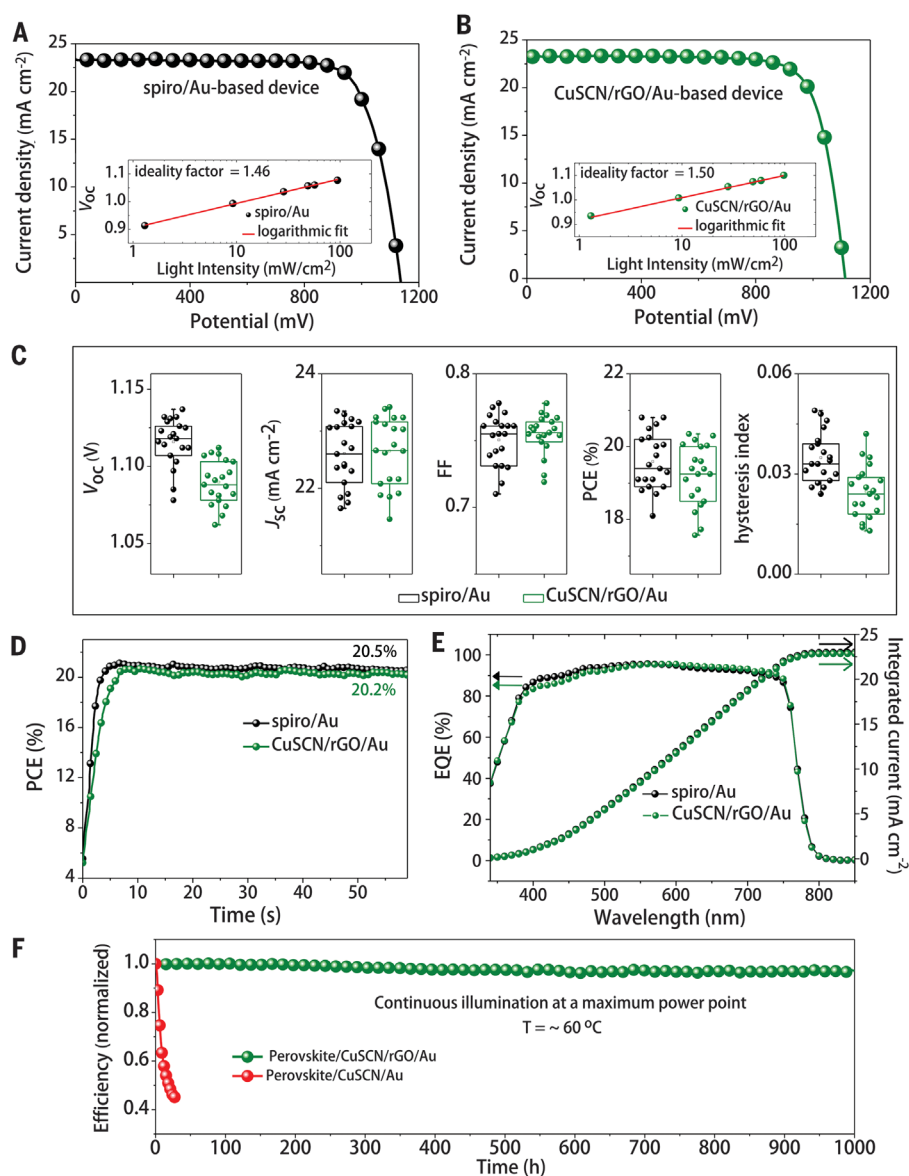


Fig. 3. Photovoltaic characterization of devices based on spiro-OMeTAD and CuSCN hole-transporting layers. (A) $J-V$ curve of the spiro-OMeTAD-based device recorded at a scan rate of 0.01 V s^{-1} ; the inset shows the open-circuit voltage V_{OC} as a function of illumination intensity with an ideality factor of 1.46. (B) $J-V$ curve of the CuSCN-based device recorded at a scan rate of 0.01 V s^{-1} ; the inset shows the V_{OC} as a function of illumination intensity with an ideality factor of 1.50. (C) $J-V$ metrics for 20 independent devices based on spiro-OMeTAD and CuSCN with an illumination area of 0.16 cm^2 . J_{SC} , short-circuit current; FF, fill factor; PCE, power conversion efficiency. (D) Maximum power point tracking for 60 s, yielding stabilized efficiencies of 20.5% and 20.2%, respectively, for spiro-OMeTAD-based and CuSCN-based devices. (E) EQE as a function of monochromatic wavelength recorded for spiro-OMeTAD-based and CuSCN-based devices; also shown are integrated current densities obtained from the respective EQE spectra. (F) Operational stability of an unencapsulated CuSCN-based device with and without a thin layer of rGO (as a spacer layer between CuSCN and gold layers), examined at a maximum power point under continuous full-sun illumination at 60°C in a nitrogen atmosphere.

spiro-OMeTAD, enabling CuSCN to be effective in its pristine form, whereas spiro-OMeTAD requires a high concentration of p-dopant and other additives (such as organic lithium salt and 4-*tert*-butylpyridine) to reach its peak performance (28).

After the successful deposition of the thin and conformal β -CuSCN layer, we investigated the photovoltaic (PV) characteristics of the devices. The PV parameters extracted from the current-voltage ($J-V$) curve (Fig. 3A) of the spiro-OMeTAD-based device yielded a short-circuit current $J_{SC} =$

23.35 mA cm^{-2} , an open-circuit voltage $V_{OC} = 1137 \text{ mV}$, and a fill factor $FF = 77.5\%$, resulting in a PCE of 20.8%. The device with CuSCN as HTM and reduced graphene oxide (rGO) as a spacer layer yielded $J_{SC} = 23.24 \text{ mA cm}^{-2}$, $V_{OC} = 1112 \text{ mV}$, and $FF = 78.2\%$, resulting in a PCE of 20.4% (Fig. 3B) (the role of rGO is discussed below). As evident from the hysteresis index values, a hysteresis effect was discernible for spiro-OMeTAD by comparing the forward and backward $J-V$ scan, but it was negligible for CuSCN (Fig. 3C) (29). Figure 3, A and B, shows that the V_{OC} yielded by CuSCN-based devices was slightly lower than that yielded by spiro-OMeTAD-based devices. To understand the cause of the V_{OC} deficit in CuSCN-based devices, we estimated the ideality factor (n), which is an indicator of the dominant recombination mechanism occurring within a working device (30). By fitting the intensity dependence of the V_{OC} curves (Fig. 3, A and B, insets) [(18), equation S1], we estimated $n = 1.46$ and 1.50 , respectively, for the spiro-OMeTAD-based and CuSCN-based devices, which indicates that the difference in the V_{OC} stemmed from marginally higher monomolecular recombination occurring within the CuSCN-based devices. J_{SC} showed linear behavior with illumination intensity in both PSCs (fig. S4).

Figure 3C summarizes the statistical analysis of PV parameters extracted from the $J-V$ curves of 20 independent devices. The high PCEs were reproducible for both spiro-OMeTAD-based and CuSCN-based PSCs. For the CuSCN-based devices, we observed an average $J_{SC} = 22.65 \pm 0.60 \text{ mA cm}^{-2}$, $V_{OC} = 1090 \pm 14 \text{ mV}$, and $FF = 0.75 \pm 0.02$, resulting in an average PCE of $19.22 \pm 0.84\%$. Similarly, for the spiro-OMeTAD-based devices, we observed an average $J_{SC} = 22.6 \pm 0.55 \text{ mA cm}^{-2}$, $V_{OC} = 1115 \pm 15 \text{ mV}$, and $FF = 0.75 \pm 0.02$, resulting in an average PCE of $19.6 \pm 0.77\%$. To determine the stabilized (scan speed-independent) PCEs, we probed the solar cells at their maximum power point under full-sun illumination (Fig. 3D). We recorded a stabilized output power corresponding to a PCE of 20.5% and 20.2% for spiro-OMeTAD-based and CuSCN-based devices, respectively, in close agreement with the $J-V$ measurements. The integrated photo-current densities obtained from the external quantum efficiency (EQE) spectra of spiro-OMeTAD-based and CuSCN-based devices agreed closely with those obtained from the $J-V$ curves (Fig. 3E), indicating that any spectral mismatch between our simulator and AM-1.5 standard solar radiation was negligible.

The long-term thermal stability of devices at high temperature has become a key problem, primarily because the diffusion of metal through a spiro-OMeTAD layer at higher temperatures leads to the degradation of the devices (22). We examined the thermal stability of CuSCN-based devices coated with a thin layer of poly(methyl methacrylate) polymer (18) at 85°C in ambient conditions in the dark. After 1000 hours, the CuSCN-based devices retained $>85\%$ of their initial efficiency (fig. S5). The formation of a uniform CuSCN film, as evident from morphological analysis, blocked

the metal diffusion (22). Long-term operational stability is a crucial requirement for future exploitations of PSC-based technology (31). Under full-sun illumination at their maximum power point, the CuSCN devices (fig. S6) showed poor photostability, losing >50% of their initial efficiency within 24 hours (Fig. 3F, red trace). Such instability of PSCs has been associated with the degradation of the CuSCN/perovskite interface (14), but atomic layer deposition of an insulating Al₂O₃ layer (~2 nm) between the perovskite and CuSCN layers did not mitigate the initial degradation (fig. S7). Instead, we introduced a thin conductive rGO spacer layer (fig. S8) between the CuSCN and gold layers, leading to excellent operational stability under full-sun illumination at 60°C. The resulting PSCs retained >95% of their initial efficiency after aging for 1000 hours, apparently surpassing the stability of spiro-OMeTAD devices recorded under similar conditions (fig. S9).

We traced the photoeffect back to the positive electrical polarization imposed on the gold when the CuSCN device is illuminated at its maximum power point or under open circuit conditions. We confirmed the occurrence of potential-induced degradation by applying a positive bias of 0.8 V to the Au contact of a CuSCN device in the dark. The results (fig. S10) illustrate the severe loss in PV performance under these conditions. When no electrical bias was applied to the cell during aging in the dark, no appreciable degradation was observed even after prolonged heating of the CuSCN devices at 85°C (fig. S5). Thus, we identify the cause of the degradation to be an electrical potential-induced reaction of gold with the thiocyanate anions forming an undesired barrier, which is different from the degradation occurring at the interfaces between perovskite and selective contacts (32). Using x-ray photoelectron spectroscopy (XPS), we confirmed the oxidation of gold (fig. S11) upon subjecting the CuSCN devices to the light soaking test over extended time periods. We conclude that the instability of PSCs is not associated with the

degradation of CuSCN/perovskite interface, as is generally believed, but rather originates mainly from the CuSCN/Au contact. The CuSCN film did not require any additives to function as an effective HTM, in contrast to PTAA and spiro-OMeTAD, which can reach their peak performance only in the presence of organic lithium salt and 4-*tert*-butylpyridine and, for the latter, also a Co(III) complex that acts as a p-dopant (4); these additives readily cross into the photoactive PSC layer and adversely affect PV performance. Our results show that PSCs using all-inorganic charge extraction layers (i.e., mesoporous TiO₂ and CuSCN) display high PCE values combined with remarkable operational and thermal stability, offering the potential for large-scale deployment.

REFERENCES AND NOTES

1. A. Kojima, K. Teshima, Y. Shirai, T. Miyasaka, *J. Am. Chem. Soc.* **131**, 6050–6051 (2009).
2. W. S. Yang *et al.*, *Science* **356**, 1376–1379 (2017).
3. H. Tan *et al.*, *Science* **355**, 722–726 (2017).
4. J. Liu *et al.*, *Energy Environ. Sci.* **7**, 2963–2967 (2014).
5. H.-S. Kim *et al.*, *Sci. Rep.* **2**, 591 (2012).
6. W. Chen *et al.*, *Science* **350**, 944–948 (2015).
7. J. A. Christians, R. C. M. Fung, P. V. Kamat, *J. Am. Chem. Soc.* **136**, 758–764 (2014).
8. I. Chung, B. Lee, J. He, R. P. H. Chang, M. G. Kanatzidis, *Nature* **485**, 486–489 (2012).
9. P. Qin *et al.*, *Nat. Commun.* **5**, 3834 (2014).
10. J. E. Jaffe *et al.*, *J. Phys. Chem. C* **114**, 9111–9117 (2010).
11. J. W. Jung, C.-C. Chueh, A. K. Y. Jen, *Adv. Energy Mater.* **5**, 1500486 (2015).
12. S. Ye *et al.*, *Nano Lett.* **15**, 3723–3728 (2015).
13. M. Jung *et al.*, *ChemSusChem* **9**, 2592–2596 (2016).
14. J. Liu *et al.*, *Adv. Mater. Interfaces* **3**, 1600571 (2016).
15. S. Ye *et al.*, *Adv. Mater.* **28**, 9648–9654 (2016).
16. V. E. Madhavan *et al.*, *ACS Energy Lett.* **1**, 1112–1117 (2016).
17. N. Yaacobi-Gross *et al.*, *Adv. Energy Mater.* **5**, 1401529 (2015).
18. See supplementary materials.
19. M. Kabešová, M. Dunaj-jurčo, M. Serator, J. Gažo, J. Garaj, *Inorg. Chim. Acta* **17**, 161–165 (1976).
20. D. L. Smith, V. I. Saunders, *Acta Crystallogr. B* **37**, 1807–1812 (1981).
21. D. L. Smith, V. I. Saunders, *Acta Crystallogr. B* **38**, 907–909 (1982).
22. Y. Han *et al.*, *J. Mater. Chem. A* **3**, 8139–8147 (2015).
23. S. D. Stranks *et al.*, *Science* **342**, 341–344 (2013).
24. L. Kong *et al.*, *Proc. Natl. Acad. Sci. U.S.A.* **113**, 8910–8915 (2016).
25. M. I. Dar *et al.*, *Sci. Adv.* **2**, e1601156 (2016).
26. G. Xing *et al.*, *Science* **342**, 344–347 (2013).
27. K. Pydzińska *et al.*, *ChemSusChem* **9**, 1647–1659 (2016).
28. W. H. Nguyen, C. D. Bailie, E. L. Unger, M. D. McGehee, *J. Am. Chem. Soc.* **136**, 10996–11001 (2014).
29. H.-S. Kim, N.-G. Park, *J. Phys. Chem. Lett.* **5**, 2927–2934 (2014).
30. K. Tvingstedt *et al.*, *Sci. Rep.* **4**, 6071 (2014).
31. F. Bella *et al.*, *Science* **354**, 203–206 (2016).
32. J. Carrillo *et al.*, *Adv. Energy Mater.* **6**, 1502246 (2016).

ACKNOWLEDGMENTS

Author contributions: N.A., M.I.D., and M.G. conceived the idea of the work; N.A. and M.I.D. designed the project and fabricated and characterized devices; M.I.D. and N.A. performed PL and SEM analysis; N.A., M.I.D., and A.H. performed the XRD measurements; A.H. and F.S. analyzed and discussed the XRD data; N.P. carried out hole mobility experiments; N.P. and M.I.D. performed light soaking measurements; M.I.D. wrote the manuscript; all the authors contributed toward finalizing the draft; S.M.Z. coordinated the project; and M.G. directed and supervised the research. Supported by Greatcell Solar SA (N.A.) and by the European Union's Horizon 2020 program through a Future Emerging Technologies (FET)-Open Research and Innovation action under grant agreement 687008 and Graphene Flagship Core1 under grant agreement 696656 (M.I.D., S.M.Z., and M.G.). We thank the European Synchrotron Radiation Facility for provision of synchrotron radiation, A. Chumakov and F. Zontone for assistance in using beamline ID10, J. Hagenlocher for assistance with XRD analysis, M. Mayer for assistance with ALD, F. Giordano and P. Yadav for helpful discussions, and P. Mettraux (Molecular and Hybrid Materials Characterization Center, EPFL) for carrying out XPS measurements. All results are presented in the main paper and supplement. We have applied for a patent on inorganic hole conductor-based PSCs with high operational stability.

SUPPLEMENTARY MATERIALS

www.sciencemag.org/content/358/6364/768/suppl/DC1
Materials and Methods
Supplementary Text
Figs. S1 to S11
Table S1
References (33, 34)

16 December 2016; resubmitted 4 August 2017
Accepted 14 September 2017
Published online 28 September 2017
10.1126/science.aam5655

Perovskite solar cells with CuSCN hole extraction layers yield stabilized efficiencies greater than 20%

Neha Arora, M. Ibrahim Dar, Alexander Hinderhofer, Norman Pellet, Frank Schreiber, Shaik Mohammed Zakeeruddin and Michael Grätzel

Science **358** (6364), 768-771.
DOI: 10.1126/science.aam5655 originally published online September 28, 2017

Transporter layers improve stability

Although perovskite solar cells can have power conversion efficiencies exceeding 20%, they can have limited thermal and ultraviolet irradiation stability. This is in part because of the materials used to extract the charge carriers (electrons and holes) from the active layer. Arora *et al.* replaced organic hole transporter layers with CuSCN to improve thermal stability. Device lifetime was enhanced when a conducting reduced graphene oxide spacer was added between the CuSCN layer and the gold electrode.

Science, this issue p. 768

ARTICLE TOOLS

<http://science.sciencemag.org/content/358/6364/768>

SUPPLEMENTARY MATERIALS

<http://science.sciencemag.org/content/suppl/2017/09/27/science.aam5655.DC1>

RELATED CONTENT

<http://science.sciencemag.org/content/sci/358/6364/732.full>
<http://science.sciencemag.org/content/sci/358/6364/734.full>
<http://science.sciencemag.org/content/sci/358/6364/739.full>
<http://science.sciencemag.org/content/sci/358/6364/745.full>
<http://science.sciencemag.org/content/sci/358/6364/751.full>
<http://science.sciencemag.org/content/sci/early/2017/11/08/science.aao5561.full>

REFERENCES

This article cites 33 articles, 8 of which you can access for free
<http://science.sciencemag.org/content/358/6364/768#BIBL>

PERMISSIONS

<http://www.sciencemag.org/help/reprints-and-permissions>

Use of this article is subject to the [Terms of Service](#)